2-26-2024

Lotic-SIPCO2: Adaptation of an open-source CO2 sensor system and examination of associated emission uncertainties across a range of stream sizes and land uses

Andrew L. Robison
Ecole Polytechnique Fédérale de Lausanne

Lauren E. Koenig
University of New Hampshire, Durham

Jody D. Potter
University of New Hampshire, Durham

Lisle E. Snyder
University of New Hampshire, Durham

Christopher W. Hunt
University of New Hampshire, Durham

LIMNOLOGY and OCEANOGRAPHY: METHODS

ASLO

Limnol. Oceanogr.: Methods 22, 2024, 191–207

doi: 10.1002/lom3.10600

Lotic-SIPCO2: Adaptation of an open-source CO_2 sensor system and examination of associated emission uncertainties across a range of stream sizes and land uses

Andrew L. Robison,[1,2]* **Lauren E. Koenig**,[2,a] **Jody D. Potter**,[2] **Lisle E. Snyder**,[2] **Christopher W. Hunt**,[3] **William H. McDowell**,[2,4] **Wilfred M. Wollheim**[2]

[1]River Ecosystems Laboratory, École Polytechnique Fédérale de Lausanne, Lausanne, Switzerland
[2]Department of Natural Resources and the Environment, University of New Hampshire, Durham, New Hampshire, USA
[3]Ocean Process Analysis Laboratory, University of New Hampshire, Durham, New Hampshire, USA
[4]Institute of Environment, Florida International University, Miami, Florida, USA

Abstract

River networks play a crucial role in the global carbon cycle, as relevant sources of carbon dioxide (CO_2) to the atmosphere. Advancements in high-frequency monitoring in aquatic environments have enabled measurement of dissolved CO_2 concentration at temporal resolutions essential for studying carbon variability and evasion from these dynamic ecosystems. Here, we describe the adaptation, deployment, and validation of an open-source and relatively low-cost in situ pCO_2 sensor system for lotic ecosystems, the lotic-SIPCO2. We tested the lotic-SIPCO2 in 10 streams that spanned a range of land cover and basin size. Key system adaptations for lotic environments included prevention of biofouling, configuration for variable stage height, and reduction of headspace equilibration time. We then examined which input parameters contribute the most to uncertainty in estimating CO_2 emission rates and found scaling factors related to the gas exchange velocity were the most influential when CO_2 concentration was significantly above saturation. Near saturation, sensor measurement of pCO_2 contributed most to uncertainty in estimating CO_2 emissions. We also found high-frequency measurements of pCO_2 were not necessary to accurately estimate median emission rates given the CO_2 regimes of our streams, but daily to weekly sampling was sufficient. High-frequency measurements of pCO_2 remain valuable for exploring in-stream metabolic variability, source partitioning, and storm event dynamics. Our adaptations to the SIPCO2 offer a relatively affordable and robust means of monitoring dissolved CO_2 in lotic ecosystems. Our findings demonstrate priorities and related considerations in the design of monitoring projects of dissolved CO_2 and CO_2 evasion dynamics more broadly.

River networks contribute significantly to global carbon budgets (Cole et al. 2007; Drake et al. 2018), and are important regional sources of carbon dioxide (CO_2) to the atmosphere (Battin et al. 2009; Butman and Raymond 2011; Raymond et al. 2013). Although recent investigations have begun to incorporate streams and rivers (i.e., lotic ecosystems) into continental CO_2 budgets (Butman et al. 2018), uncertainties in our understanding of the temporal dynamics of lotic CO_2 concentration and emissions limit robust scaling across time (van Geldern et al. 2015). Until roughly the last decade, measurement of CO_2 concentration in aquatic systems was restricted to grab sampling (Koschorreck et al. 2021) or estimation through alkalinity titration (Butman and Raymond 2011). However, sensors capable of measuring CO_2 in situ are now available and allow high-frequency data collection at timescales relevant to hydrologically and biogeochemically dynamic lotic ecosystems (Emery and Greenville 2015; Rode et al. 2016). Still, the usefulness of

*Correspondence: andrew.robison@epfl.ch

Author Contribution Statement: ALR and WMW conceptualized the study. ALR, LEK, JDP, LES, and CWH designed and constructed the sensors systems. ALR. LEK, JDP, LES performed field work, sample collection, and laboratory analyses. ALR, LEK, and JDP performed data quality control and analysis. ALR performed data analysis and led manuscript development. All authors contributed to the final version of the manuscript. ALR, LEK, WHD, and WMW secured funding for the research.

Additional Supporting Information may be found in the online version of this article.

[a]Present address: U.S. Geological Survey, Water Mission Area, Reston, Virginia, USA

high-frequency dissolved CO_2 measurements in estimating longer-term seasonal or annual emissions from streams remains unclear, as do uncertainties and accuracy of sensor methods in general.

Lotic CO_2 varies at temporal scales ranging from minutes to years. The causes of this variation include discharge variability (Natchimuthu et al. 2017), in-stream metabolism (Rocher-Ros et al. 2020), anthropogenic disturbance (Marescaux et al. 2018), and climate variability (Sawakuchi et al. 2017). On daily timescales, patterns of in-stream photosynthesis and respiration are often important in driving CO_2 maxima during the night (Rocher-Ros et al. 2020; Gómez-Gener et al. 2021). This diel variation is not universal across streams (Crawford et al. 2017) and can be interrupted by disturbances such as storm events (Peter et al. 2014). However, changes in discharge also do not affect CO_2 concentrations uniformly across streams (Liu and Raymond 2018). Still, discharge variability can cause large changes in pCO_2 on hourly to seasonal timescales, for example from less than 10 μM CO_2 to more than 800 μM CO_2 within a single day during a storm event (Wallin et al. 2020).

The development and proliferation of accurate, affordable, lotic pCO_2 sensors offers novel approaches to understand mechanisms controlling such CO_2 dynamics. For example, pairing aquatic CO_2 and oxygen sensors has provided quantitative insights into stream metabolism (Rocher-Ros et al. 2020), aquatic-terrestrial linkages (Marzolf et al. 2022), and in large river systems (Haque et al. 2022). Tracking diel patterns of these gasses allows for the partitioning of aquatic and terrestrial sources of CO_2 to a stream, highlighting the potential loss of terrestrially derived carbon through the aquatic network. Similarly, examination of high-frequency aquatic CO_2 data with spectral analyses has shown the importance of aquatic biological processes in regulating CO_2 concentration and emissions from sub-daily to seasonal timescales (Riml et al. 2019). Concentration-discharge dynamics explored using high-frequency CO_2 sensors have also provided insights into temporally variable sources of CO_2 to streams and how these change during storm events (Dinsmore and Billett 2008; Dinsmore et al. 2013). These scientific advances afforded by high-frequency measurements highlight the utility of using sensors to fully contextualize CO_2 dynamics in streams and rivers. Still, the necessity of high-frequency measurements in accurately capturing average seasonal emission rates remains understudied, as do the sources and magnitude of uncertainties associated with different sampling frequencies.

In lotic ecosystems, CO_2 sensors have typically either been land- or boat-based instrumentation that relies on headspace equilibrium in dry conditions (e.g., Peter et al. 2014; Sawakuchi et al. 2017) or submergible sensors fitted with gas permeable membranes (e.g., Johnson et al. 2010; Rocher-Ros et al. 2020; Reed et al. 2021). The infrastructure necessary for land- or boat-based instrumentation is typically limiting for long term deployments, and energy demands are typically much higher than for submergible sensors (Yoon et al. 2016). Submergible sensors include the GMT220 sensor (Vaisala, Finland), the eosGP CO_2 concentration probe (Eosense, Dartmouth, Canada), the CO2-Pro sensor (ProOceanus Systems Inc., Nova Scotia, Canada), and low-cost, user-constructed models (Blackstock et al. 2019), all of which rely on diffusion of CO_2 across a gas permeable membrane (Johnson et al. 2010). However, the equilibration time of membrane enclosed sensors (> 30 min in low flow conditions) is typically longer than that of headspace equilibrium methods (< 10 min and independent of flow conditions), which reduces the temporal resolution of membrane enclosed sensors when CO_2 variation is less than the equilibration time (Yoon et al. 2016). In addition, submergible sensors often rely on calibration in dry laboratory conditions, giving some uncertainty to sensor measurement effects from pressure, temperature, and humidity (Welles and McDermitt 2005) and potential condensation from internal electronics within the headspace (Blackstock et al. 2019).

The limitations of each of these methods suggest that there is an opportunity to improve CO_2 sensor capabilities in lotic environments which balance the relative affordability and adaptability of submergible sensors with the responsiveness of headspace equilibrium methods. The objective of this study was to examine CO_2 emissions from lotic environments using the novel, low-cost SIPCO2 method which has previously only been applied in estuarine ecosystems (Hunt et al. 2017). We first describe the adaptation of the SIPCO2 to lotic environments, and then analyze the uncertainty in estimating CO_2 emissions using these sensors. Because numerous studies have explored the accuracy of similarly designed aquatic pCO_2 sensors in detail (Yoon et al. 2016; Hunt et al. 2017; Blackstock et al. 2019; Lee et al. 2022), we instead explore the effectiveness of this headspace sensor systems in estimating CO_2 emissions from several lotic systems spanning a range of streamflow and land use conditions, biofouling potential, and other environmental factors. While some high-frequency dissolved CO_2 datasets have been published from lotic ecosystems, no study that we are aware of has analyzed the utility and uncertainty of using sensors to estimate CO_2 emissions from streams and rivers over longer time scales. As such, validation of a low-cost in situ sensor system relying on headspace equilibrium has the potential to greatly expand high-frequency measurements of CO_2 in aquatic systems broadly.

Methods

We adapted a relatively inexpensive (~ 500 USD) and user-built headspace equilibrium-based pCO_2 sensor for deployment in lotic ecosystems, the lotic-SIPCO2. The original SIPCO2 design (Hunt et al. 2017) and published adaptations (Lee et al. 2022) are specified for marine and estuarine deployments, thus moving into lotic ecosystems necessitated adaptation for variable flow and stream stage. Using these sensors,

the concentration of dissolved CO_2 was measured at 15-min intervals and validated against grab samples in 10 streams and rivers ranging in watershed size from 0.4 to 476.7 km^2 over the course of 1–6 yr (2015–2020) during ice-free months (approximately May to October). Combined with measurements of water temperature, estimates of discharge, hydraulic geometry, gas exchange estimates, and either the measured or estimated concentration of CO_2 in the air, we estimated CO_2 emissions from each stream or river reach over the course of each record. We then evaluated the sensitivity of the estimated CO_2 emission estimates in relation to uncertainty in each of these input parameters. Finally, given this calculated uncertainty, we examine the sampling frequency necessary to accurately represent seasonal estimates of CO_2 emissions.

Site description

Ten streams and rivers in New Hampshire and Massachusetts were studied (Fig. 1), ranging from small headwater streams draining various land covers to two larger, main stem river sites (Table 1). Five sites were part of the New Hampshire EPSCoR High-Intensity Aquatic Network (Koenig 2017): Paradise Brook, the outlet to the reference Watershed 3 at Hubbard Brook Experimental Forest (HB), Wednesday Hill Brook (WHB), Trout Pond Brook (TPB), Dowst Cate Forest (DCF) stream, and the Lamprey River (LMP) at the outflow of the Lamprey River Reservoir. Three sites are part of the Plum Island Ecosystems Long-Term Ecological Research program (Morse and Wollheim 2014): Cart Creek (CC), Sawmill Brook (SB), and the Ipswich River (IR) above the reservoir created by the South Middleton dam. The remaining two sites are part of long-term monitoring projects of the Oyster River watershed near Durham, NH (Wollheim et al. 2017): College Cook (CB) and Dube Brook (DB). Eight of the 10 sites are 1st- or 2nd-order streams, with watersheds ranging from 0.4 km^2 at HB to 7.0 km^2 at DCF. A 4th-order river, IR drains approximately 115 km^2, and LMP is a 6th-order system draining 477 km^2. Land use varies from nearly complete forest cover (> 99%) at HB, to large wetland influence (> 55%) at DB, CC, and IR, to suburban watersheds at CB, SB, and IR (< 20% impervious surfaces). The slope of the sites is generally shallow (0.040 km km^{-1} or less), apart from the montane HB (0.141 km km^{-1}).

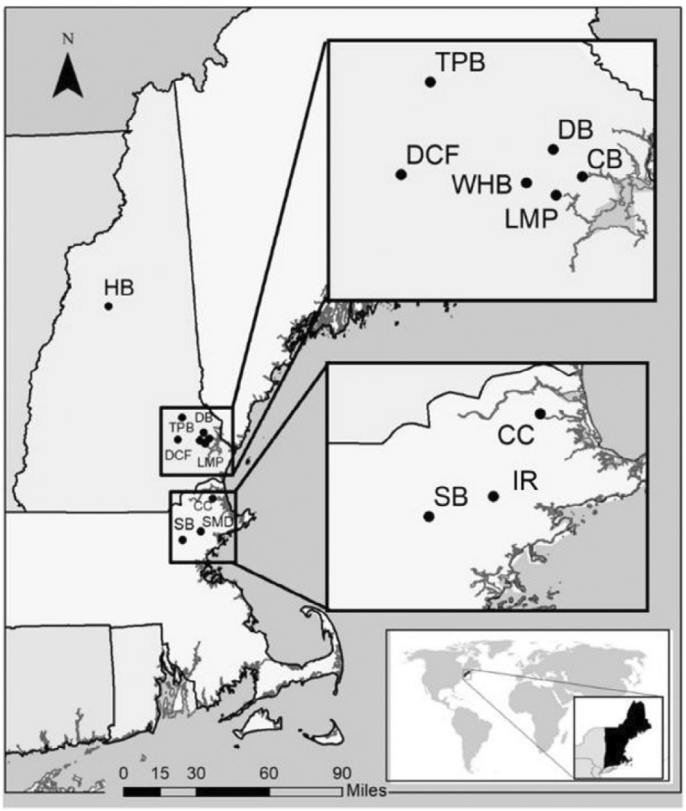

Fig. 1. Map of 10 monitoring locations in streams and rivers of Massachusetts and New Hampshire, USA.

Sensor system and adaptation for lotic ecosystems

Dissolved CO_2 was measured at each site with the SIPCO2 method (Hunt et al. 2017). The SIPCO2 (Fig. 2) is a relatively inexpensive, in situ pCO_2 sensor in which a non-dispersive infrared (NDIR) detector (SenseAir K30, ASCII model, Delsbo, Sweden) in an enclosed housing is paired with a continuously operating air pump (Brushless pump, MPU3671-NMP05, KNF Neuberger) to produce air–water equilibration in an enclosed headspace (Fig. 2a). Briefly, headspace air is re-circulated below the water surface by the pump. The bubbles equilibrate with the surrounding water as they rise, including dissolved gases such as CO_2. As the bubbles break into the sensor system housing, the released air rises through the pipe toward the NDIR detector. The sensor housing and tube constitute the headspace volume, which is reduced by the materials contained in this space. The cost of construction of a single sensor was approximately 500 USD as of 2018, and takes approximately 3 d to construct once trained, including the drying time of the silicone sealant. Sensors were powered by 12.6 V batteries outfitted with 10 or 25 W solar panels.

Sensors are controlled with an Arduino Nano microcontroller (Arduino) or CR1000 dataloggers (Campbell Scientific). The manufacturer-specified range of the K30 1% detectors is 0 to 10,000 ppmv CO_2, with an accuracy of ± 30 ppmv CO_2 and ± 3% of the measured concentration. The detector is calibrated with 0 and 400 ppmv CO_2 standard gases using a vendor-supplied software control program (Gaslab, Gaslab.com). Possible drift in sensor measurement was assessed at the end of the monitoring season beginning in 2018. Sensor measurements were made using four standard gases with 0, 394, 838, and 1990 ppmv CO_2, assuming full calibration at the beginning of the season. The accuracy of these measurements was measured by simple linear regression, with significant sensor drift indicated by a slope different from 1 or an intercept different from 0.

We make three major modifications to the original construction and design described by Hunt et al. (2017). First, equilibration time of the SIPCO2 is inherently dependent on

Table 1. Watershed and stream characteristics of monitoring sites, obtained from the National Hydrography Dataset (Wieczorek et al. 2018).

Site	Watershed area (km^2)	NHD stream order	% Forest	% Wetland	% Impervious	Stream slope (km km^{-1})	Length of CO_2 record (yr)
HB	0.4	1	99.3	0.0	0.0	0.141	5
WHB	1.0	1	58.1	6.8	5.6	0.040	6
CB	2.3	1	20.8	0.7	28.4	0.038	3
DB	3.3	1	59.4	17.3	4.8	0.028	3
CC	3.9	1	55.3	18.6	8.2	0.021	3
SB	4.1	2	13.7	4.3	24.6	0.034	3
TPB	4.1	1	88.6	6.1	0.0	0.010	5
DCF	7.0	2	71.9	11.7	0.4	0.037	6
IR	106.7	4	31.5	20.5	20.7	0.010	1
LMP	476.7	6	67.4	12.4	1.8	0.009	2

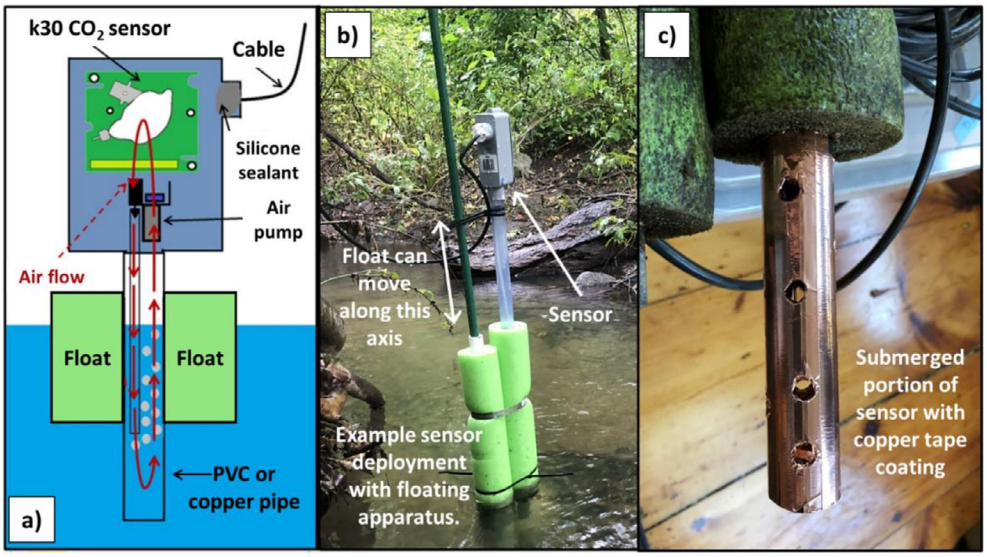

Fig. 2. (**a**) Lotic-SIPCO2 sensor design, adapted from Hunt et al. (2017). (**b**) Example deployment of lotic-SIPCO2 sensor with novel float design. (**c**) Image of the submerged portion of a lotic-SIPCO2 sensor with copper tape coating to minimize biofouling.

the volume of the headspace. Reduction of this volume by shortening of the polyvinyl chloride (PVC) tube to roughly 50 cm reduced equilibration to approximately 15 min (Supporting Information Fig. S1). As such, measurement of pCO_2 at 15-min intervals was possible, matching commonly used intervals for many hydrologic and water quality monitoring variables. At each 15-min interval, the K30 sensor made 30 individual measurements over 1 min (i.e., at 2-s intervals), and the mean and standard deviation of these values were recorded.

Second, the SIPCO2 sensors must be anchored in place in lotic ecosystems to counteract downstream transport. One solution to this was to anchor the sensors to trees adjacent to the stream, with the tubing submerged in the water. This was done at HB, WHB, TPB, DCF, and LMP, with adjustments of the vertical placement of the sensor to account for seasonal changes in stream stage. At CB, DB, CC, SB, and IR, a metal stake was anchored in the stream channel and the sensors were attached (Fig. 2b). To account for changes in stage during storm events, a float system was developed in which the sensor system could move up and down the metal stake while maintaining relatively stable buoyancy and headspace volume.

Finally, biofouling on the submerged portions of the sensors affected accurate measurement of pCO_2. Two methods were adopted to limit biofouling following other submergible sensor applications (e.g., Wallin et al. 2020). First, at WHB and LMP, the PVC pipe was replaced with a copper pipe. Second, at CB, DB, CC, SB, and IR, copper tape was applied to the inside and outside of the submerged PVC portion (Fig. 2c). Both applications of copper appeared to prevent or greatly reduce biofouling. Biofouling was limited or absent at HB, DCF, and TBP. Prior to these solutions, or for the sites with minimal biofouling, the

inside and outside of the submerged PVC pipe was cleaned regularly during site visits with a brush. Periods of record affected by biofouling were removed from analysis.

Dissolved CO_2 sampling

Surface water samples were collected regularly (weekly to monthly) at each site for measurement of pCO_2 using acid-washed 60-mL polypropylene syringes fitted with three-way stopcocks with luer lock fittings. Syringes were filled with stream water, and then cleared of air bubbles by inverting and expelling the bubbles and water (Magen et al. 2014). The syringes were then expelled to retain 30 mL of stream water and sealed. Samples were preserved on ice in the dark and returned to the laboratory within 8 h of collection. The lability of organic carbon from these locations has previously been determined to be low (uptake velocity = 14 m yr^{-1}; Wollheim et al. 2015), thus we assume minimal respiration within the syringe. Comparison of field and laboratory equilibrated samples indicates no bias in methodology, suggesting stability of our samples prior to equilibration (Supporting Information Fig. S2). In the laboratory, 30 mL of helium was added to each syringe to achieve a 1 : 1 ratio of sample water to air, and syringes were shaken for 3 min to equilibrate gases between the headspace and water (Mulholland et al. 2004). The resulting headspace gas was then injected into evacuated glass vials sealed with a rubber septum until analyzed.

Samples were analyzed for CO_2 concentration using a thermal conductivity detector on a Shimadzu GC-2014 gas chromatograph (Shimadzu). Standards of 400, 838, 1990, and 6000 ppmv CO_2, as well as helium as a 0 ppmv gas, were used for the calibration curve. The concentration of CO_2 in the sample headspace (ppmv) was converted to dissolved gas concentration in the water sample (μM) using Henry's law constant, temperature, and atmospheric pressure (Herreid et al. 2020). The accuracy of the lotic-SIPCO2 was evaluated by comparing measurements to grab samples of dissolved CO_2 using simple linear regression with an intercept of zero. The slope of the regression was evaluated for its difference from one, and the coefficient of determination from simple linear regression (r^2) and the normalized root mean squared error (NRMSE) were used to compare sensor measurements to grab samples. The NRMSE is the root mean squared error normalized by the range of observed data, with values close to 0 being indicative of better fit (Pontius et al. 2008; Ranatunga et al. 2017). Here, we use the range of sensor measured values at a site because of the larger coverage compared to the grab samples. We report the NRMSE as a percentage.

Estimation of CO_2 emissions

The flux of CO_2 to the atmosphere (F_{CO_2}, g CO_2-C m^{-2} d^{-1}) was calculated as,

$$F_{CO_2} = k_{CO_2} \times \left(CO_{2,water} - CO_{2,eq}\right) \quad (1)$$

where k_{CO_2} (m d^{-1}), the gas transfer velocity for CO_2, is multiplied by the difference in measured CO_2 concentration ($CO_{2,water}$, g m^{-3}) and the equilibrium concentration ($CO_{2,eq}$, g m^{-3}). The equilibrium concentration of CO_2 is the product of atmospheric CO_2 concentration ($CO_{2,air}$, μatm) and Henry's Law constant (K_{H,CO_2}, mol L^{-1} atm^{-1}),

$$CO_{2,eq} = CO_{2,air} \times K_{H,CO_2} \quad (2)$$

The constant K_{H,CO_2} is calculated as,

$$K_{H,CO_2} = k_H^{\circ} \exp\left(k_H^T \left(\frac{1}{T} - \frac{1}{298.15}\right)\right), \quad (3)$$

where k_H° (0.035) is Henry's law constant for solubility of CO_2 in water at 298.15 K, k_H^T (2400) is the temperature dependence constant for CO_2, and T is the water temperature (K).

At four of the sites (HB, WHB, TPB, and DCF), a K30 CO_2 analyzer was deployed near the stream and measured the concentration of CO_2 in the air ($CO_{2,air}$). These sensors were calibrated in the same manner as described previously. Where these data were not available, or where there were missing data, the median of all $CO_{2,air}$, 422 ppmv, was used (Supporting Information Fig. S3). Sensor measurements were converted to molar concentration using Henry's law to account for atmospheric pressure and water temperature.

The gas exchange rate for CO_2, k_{CO_2} (m d^{-1}) was calculated as,

$$k_{CO_2} = \left(\frac{SC_{CO_2}}{600}\right)^{1/2} / k_{600} \quad (4)$$

where SC_{CO_2} is the Schmidt number for CO_2 at a given water temperature and k_{600} is the gas transfer velocity (m d^{-1}) standardized for a Schmidt number of 600 (Raymond et al. 2012). We estimated k_{600} (m d^{-1}) for each reach based on an empirical relationship following Raymond et al. (2012):

$$k_{600} = aS^bV^c \quad (5)$$

where S is the channel slope (unitless), V is the water velocity (m s^{-1}), and a (1162 ± 192), b (0.77 ± 0.028), and c (0.85 ± 0.045) are constants. This formula was selected as it had the strongest correlation with measurements of gas exchange in the streams of Strahler order one and two in previous studies (Koenig 2017; Robison et al. 2022). The slope of each stream reach was found using high-resolution digital elevation models. Predictive relationships for changes in velocity at a site (V, m s^{-1}) were made using the equations for scaling of stream geometry at a site (Knighton 1998),

$$V = mQ^n \quad (6)$$

where Q is discharge ($m^3\ s^{-1}$) and the exponent n is 0.4. The coefficient m is derived for each site using the mean discharge (Q_{mean}) and mean flow velocity (V_{mean}), where V_{mean} is derived from the relationship across streams and rivers of various sizes (Raymond et al. 2012),

$$V_{mean} = \exp(0.285 \ln(Q_{mean}) - 1.64) \quad (7)$$

The resulting coefficients, m, ranged from 0.32 at the smallest sites to 0.18 at the largest sites.

Discharge was available from long-term monitoring projects for HB, WHB, TPB, and DCF (Koenig et al. 2017), CB and DB (Wollheim et al. 2017), and CC and SB (Morse and Wollheim 2014). Site-specific stage-discharge rating curves were developed for each site, where continuous stage loggers (HOBO Water Level U20L-04, Onset) are related to discharge measurements. Discharge measurements were made using a combination of cross-sectional velocity measurements using handheld acoustic Doppler velocimeters (FlowTracker2, SonTek) with the mid-section method (Pelletier 1988) and dilution gaging of salt slug injections (Richardson et al. 2017). While discharge measurements were made across a variety of flow conditions, larger flows associated with storms at times exceeded the maximum level of discharge measurement (< 1.5% of data record across all sites). For IR and LMP, our sampling locations are located less than 1 km upstream of USGS gages 01101500 and 01073500, respectively. Watershed area increases minimally between the sampling location and USGS gage (< 0.5%), thus we use the discharge data from these two USGS stations without adjustment.

All data analysis and statistical methods were performed in MATLAB and Statistics Toolbox Release 2022a (The MathWorks, Inc.). Median pCO_2 and F_{CO2} were compared to land cover categories using simple linear regression, with the coefficient of determination (r^2) used to measure goodness-of-fit. Some direct measurements of the gas transfer velocity at the 1st- and 2nd-order systems were measured using argon as a conservative gas tracer (Hall and Madinger 2018). We use these direct measurements as a means of examining the general accuracy of the estimated gas transfer velocity from Eqs. 5–7 (Supporting Information Fig. S4).

Sensitivity and uncertainty analyses

Estimation of F_{CO2} from the streams relied on measurements and equations with known and unknown levels of uncertainty. Thus, the propagation of this uncertainty was critical to understanding both the accuracy of the resulting F_{CO2} estimates as well as the sensitivity of F_{CO2} to input parameters. For example, sources of observation uncertainty included sensor accuracy. The K30 CO_2 sensor has a manufacturer's accuracy of ± 30 ppm and 3% of the measured value. Similarly, the parameters of the k_{600} equation each have associated uncertainty (Raymond et al. 2012).

To understand the influence of each input parameter on the calculation of F_{CO2}, we implemented a Monte Carlo simulation with 1000 iterations and defined uncertainty ranges around each input parameter. For each of these parameters and at each stream, the theoretical value was set as the median during the period 01 June 2019 through 01 September 2019. This period was selected because sensor adaptations were applied at this time, and the data record is complete for 9 of the 10 streams. A normal distribution was then generated for each input variable using either a known standard deviation or by conservatively assigning a percent uncertainty (Table 2). For variables without defined uncertainty, we set the standard deviation to 10% based on the relative confidence in the measurement of these variables (discharge, temperature, slope; Yanai et al. 2015), and 20% for all others (scaling parameters in Eq. 6) where confidence is not well defined. The standard deviation from the Monte Carlo simulations was used to determine the uncertainty of F_{CO2}. A larger standard deviation thus indicated greater uncertainty at a given stream. In addition, the sensitivity of F_{CO2} to each input parameter was evaluated by correlation analysis using the Pearson correlation coefficient (r) at each stream. High values of r indicate greater sensitivity of F_{CO2} to an input parameter.

This sensitivity analysis is not an exhaustive examination of uncertainty within our study system. Instead, it is a rough assessment of which parameters are likely to contribute the most to stream F_{CO2} uncertainty in studies using high-frequency sensors and under which conditions these parameters are influential. For example, we do not attempt to determine an exact uncertainty by comparing measurements of dissolved CO_2 concentration with sensor measurements. The use of

Table 2. Variables used in the estimation of F_{CO2} uncertainty. The mean value for each variable was either measured directly by sensors, estimated by equations and ratings curves described in the text, or set as coefficients and exponents in equations of gas exchange and hydraulic geometry. The variables m and n are the coefficient and exponent of Eq. 6, respectively. The variables a, b, and c, are the coefficient, 1st exponent, and 2nd exponent from Eq. 5, respectively, with uncertainty defined in Raymond et al. (2012).

Variable	Mean	SD (%)
$CO_{2,water}$ (ppm)	Measured	± 30% ± 3%
$CO_{2,air}$ (ppm)	Measured	± 30% ± 3%
Discharge (L s^{-1})	Estimated	10%
Temperature (°C)	Measured	10%
Slope	Estimated	10%
m	Estimated	20%
n	0.4	20%
a	1162	192
b	0.77	0.028
c	0.85	0.045

pre-defined and generalized quantities, such as the manufacturer's specifications, provide a more impartial approach to assess general patterns across sites. This could be viewed as a conservative estimate of uncertainty, given the SIPCO2 design has been shown to be more accurate than manufacturer's specifications (Hunt et al. 2017; Lee et al. 2022). The resulting sensitivities provide a framework to potentially differentiate which parameters contribute to uncertainty and under which conditions, such as in smaller and larger streams or under high or low CO_2 saturation conditions. As such, the exact uncertainty of each input parameter is not critically important, but rather provides the necessary structure on which to assess the sensitivity.

We also examined the impact of sampling frequency on estimating median F_{CO2} by randomly sampling the sensor time series at frequencies ranging from twice daily to once monthly. We first established the median F_{CO2} for each site as that calculated using the full sensor-based F_{CO2} dataset for the period 01 June 2019 through 01 September 2019 ($F_{CO2,theoretical}$). Then, a random value F_{CO2} was selected from the 15 min time series at the corresponding interval, for example, two random sample points per day. A median F_{CO2} value was then re-calculated from the respective subsampled time series ($F_{CO2,simulated}$). This process was repeated 1000 times for each sampling frequency to create a distribution of possible estimates. The distribution of $F_{CO2,simulated}$ for each respective subsample was then compared to $F_{CO2,theoretical}$ to determine what fraction of simulations fall within the 90% confidence bounds as determined by the uncertainty analysis described previously. While this uncertainty in $F_{CO2,theoretical}$ also applies to each $F_{CO2,simulated}$, we do not incorporate $F_{CO2,simulated}$ uncertainty into this analysis of sampling frequency. Instead, we only consider the uncertainty in $F_{CO2,theoretical}$ in determining what fraction of $F_{CO2,simulated}$ are accurate.

We then examined the impact of nighttime sampling on estimating accurate median F_{CO2}. Following Gómez-Gener et al. (2021), we calculated the median F_{CO2} from each site between the hours of 12 : 00 and 17 : 00 for daytime values, and between 00 : 00 and 05 : 00 for nighttime samples. We then replicated the random sampling regime above using only samples between the hours of 12 : 00 and 17 : 00 again. We again define an accurate $F_{CO2,simulated}$ as one that falls within the 90% confidence interval of $F_{CO2,theoretical}$.

Results

Sensor performance

During deployment, sensors functioned approximately 70–100% of the time across sites and seasons. The most common reason for malfunction was low battery power, caused primarily by the power demand of the continuously operating pumps. This issue was resolved in the short term by replacing the battery regularly, and in the longer term by increasing the size of attached solar panels. Occasionally, lotic-SIPCO2 sensors were damaged or unmoored during high-flow events, resulting in either sensor failure or loss of connection with the stream. Recorded data were removed for what was deemed to be likely inaccurate measurements due to high biofouling during years of measurements prior to copper tubing and taping applications. In addition, in 2020, a severe drought affecting the area also caused cessation of flow in some streams (e.g., DB and SB). When flows are low enough, the sensors cannot be adequately submerged and thus are not sealed to the stream water environment.

Dissolved CO_2 measurements made by lotic-SIPCO2 exhibited relative consistency with grab measurements (median $r^2 = 0.69$); however, error metrics were mixed (median NRMSE = 12.2%; Fig. 3). Correlation (r^2) between sensor measurements and grab samples among sites ranged from 0.27 to 0.93, with $r^2 > 0.5$ at eight sites. The slope of these correlations was not significantly different than 1 at 8 of 10 sites. The correlation and slope comparison generally suffer when many grab samples were available (e.g., at WHB and DCF). The NRMSE ranged from 3.2% at SB to 19.7% at LMP, with four locations exhibiting an NRMSE below 10%, and nine below 15%.

Drift analysis in 2018 indicated seven of nine sensors did not drift with respect to their slope, and eight of nine with respect to their intercept (Supporting Information Table S1). That is, sensor accuracy was fully maintained throughout the 2018 monitoring season for seven of nine sensors. At the two sites where drift was detected, TPB and LMP, corrections were made by applying the altered relationship linearly over the course of the monitoring period. Drift corrections, following these same methods, were made at three sites in 2019 and one in 2020.

CO_2 concentration, emissions, and uncertainty

The median dissolved CO_2 concentration measured with lotic-SIPCO2 sensors across all sites and time was $64.6 \pm 2.9\ \mu M\ CO_2$ (Table 3; Fig. 4a). Uncertainty here is defined by the manufacturer's specification. The median percent saturation at all sites was above 100%, indicating streams were typically oversaturated with respect to CO_2. At four sites (WHB, CC, SB, and IR), CO_2 was always supersaturated during the monitoring period; at five sites (CB, DB, TPB, DCF, and LMP), CO_2 was supersaturated during at least 95% of monitoring period; and at HB, CO_2 was supersaturated approximately 70% of the time. On average, the 2nd-order, suburban stream, SB, had the highest median CO_2 concentration ($136 \pm 5.9\ \mu M\ CO_2$), whereas a steep, forested headwater stream, HB, had the lowest ($26.6 \pm 1.1\ \mu M\ CO_2$). The highest instantaneous measurement of pCO_2 was $311 \pm 13\ \mu M\ CO_2$ at CC, and the lowest was $11.1 \pm 2.3\ \mu M\ CO_2$ at LMP, which is at the outflow of a reservoir. Watershed percent forest cover most strongly correlated with median CO_2 concentration ($r^2 = 0.61$), with higher forest cover corresponding to lower median CO_2 concentration. Combining watershed percent wetland and impervious cover explained more variance ($r^2 = 0.80$), and exhibited positive correlation.

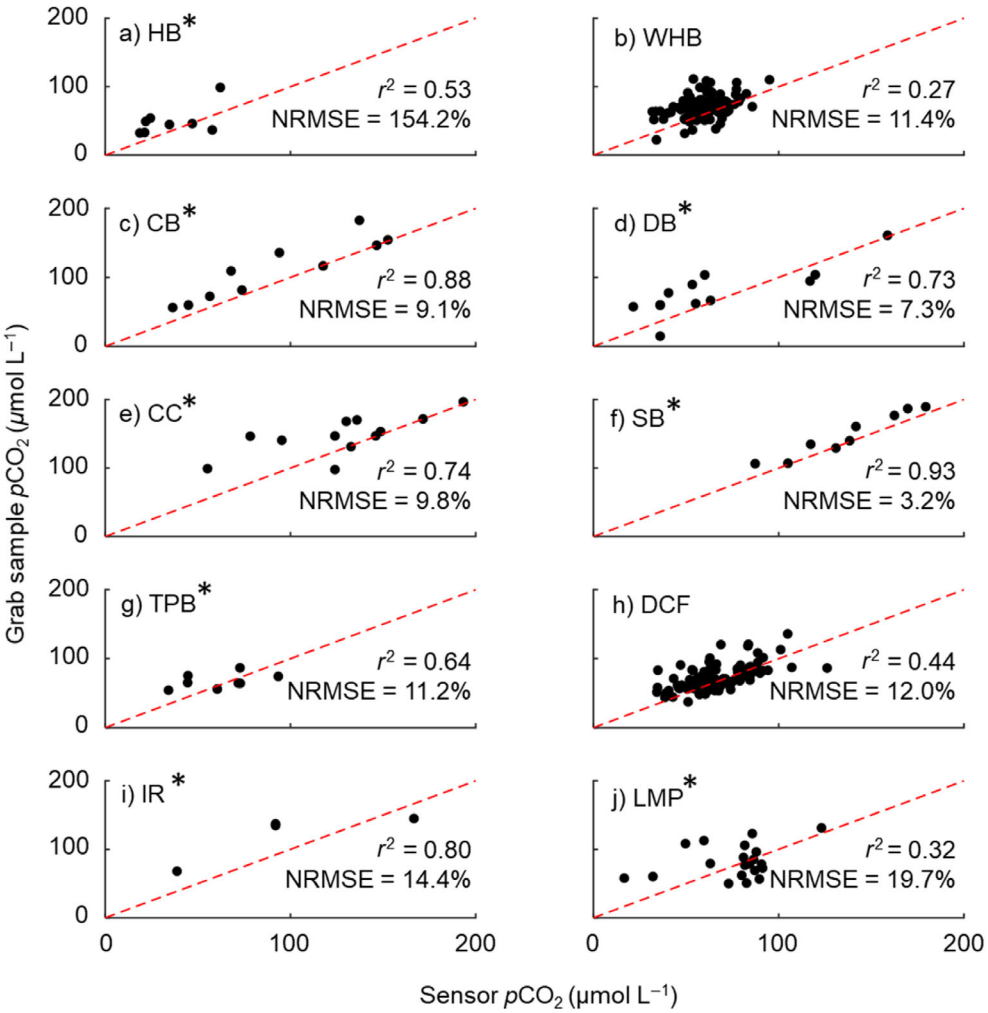

Fig. 3. Comparison of dissolved CO_2 measurements by lotic-SIPCO2 compared to by grab sampling and analysis on a gas chromatograph. The dashed red line displays the 1 : 1 relationship. Site names marked with asterisk symbols are significant correlations ($p < 0.05$). NRMSE is the normalized root mean square error, shown as a percentage.

The range of predicted gas exchange rates, k_{CO2}, was generally greater within a single site than when comparing the median values across sites (Table 3; Fig. 4b). The largest median k_{CO2} was 15.9 ± 6.4 m d^{-1} at the montane HB; and the lowest median k_{CO2} was 4.4 ± 1.7 m d^{-1} at CC, a relatively small stream with a shallow slope. Uncertainty in the gas exchange rate is defined by ranges in the scaling of velocity with discharge and the gas exchange rate from velocity and slope. The smallest range of predicted k_{600} was 12.9 ± 5.2 m d^{-1} at TPB (1.8–14.7 m d^{-1}) where the stream drains the outlet of a lake and extended up to 93.4 ± 37.8 m d^{-1} at the comparably steep HB (3.5–96.9 m d^{-1}). Measured k_{600} from previous studies (Koenig 2017; Robison et al. 2022) and modeled rates in this study were significantly correlated ($r^2 = 0.43$; $p < 0.01$), but this comparison includes only a small portion (1–12 m d^{-1}) of the total modeled range (Supporting Information Fig. S4).

Emissions of CO_2 (F_{CO2}) were predominantly positive, that is, the streams were net sources of CO_2 to the atmosphere (Fig. 4c). The median F_{CO2} across all sites was 3.3 ± 1.4 g C m^{-2} d^{-1}. The highest median F_{CO2} at an individual site across the entire monitoring period was at IR (10.2 ± 4.3 g C m^{-2} d^{-1}), and the lowest was at HB (0.8 ± 0.4 g C m^{-2} d^{-1}). Uncertainty is defined by the Monte Carlo simulation described previously. The highest instantaneous F_{CO2} estimated was 71.6 ± 29.9 g C m^{-2} d^{-1} at SB and 64.1 ± 25.7 g C m^{-2} d^{-1} at CB, both of which occurred during storms in these suburban streams. The median F_{CO2} across each monitoring year was positive at all sites across years. The lowest single annual median rate of emission was 0.1 ± 0.3 g C m^{-2} d^{-1} at HB in 2019. Periods of CO_2 uptake (negative F_{CO2}) were predicted to occur at 6 of the 10 streams, when the streams were undersaturated with respect to CO_2. Estimated emissions during these

Table 3. Summary statistics of dissolved CO_2 as measured by lotic-SIPCO2, the gas exchange velocity for CO_2 (k_{CO2}), and the estimated rate of CO_2 emission (F_{CO2}). Median values are listed with the interquartile range in parenthesis. Sites are listed in order of watershed area, from smallest to largest.

	Dissolved CO_2				
Site	μM	% Saturation	% Time below saturation	k_{CO2} (m d^{-1})	F_{CO2} (g C m^2 d^{-1})
HB	26.6 (21.4)	164 (122)	32.6	15.9 (9.8)	0.8 (2.3)
WHB	62.8 (15.5)	288 (78)	0.0	7.8 (3.1)	3.3 (1.9)
CB	85.2 (50.3)	506 (319)	1.4	6.7 (2.7)	5.7 (3.1)
DB	86.4 (88.2)	571 (515)	0.3	5.9 (3.2)	4.3 (3.8)
CC	136 (50.8)	734 (316)	0.0	5.6 (3.6)	5.8 (4.2)
SB	136 (47.2)	812 (345)	0.0	8.1 (3.6)	9.0 (4.6)
TPB	50.6 (38.4)	280 (203)	4.0	4.4 (2.2)	1.6 (1.1)
DCF	65.5 (24.2)	338 (155)	0.7	11.6 (5.8)	4.6 (2.8)
IR	132 (79.3)	797 (559)	0.0	9.6 (4.3)	10.2 (3.6)
LMP	80.7 (32.5)	417 (232)	1.8	11.0 (6.7)	5.1 (3.6)
All	64.6 (36.7)	307 (223)	4.9	7.7 (6.0)	3.3 (3.6)

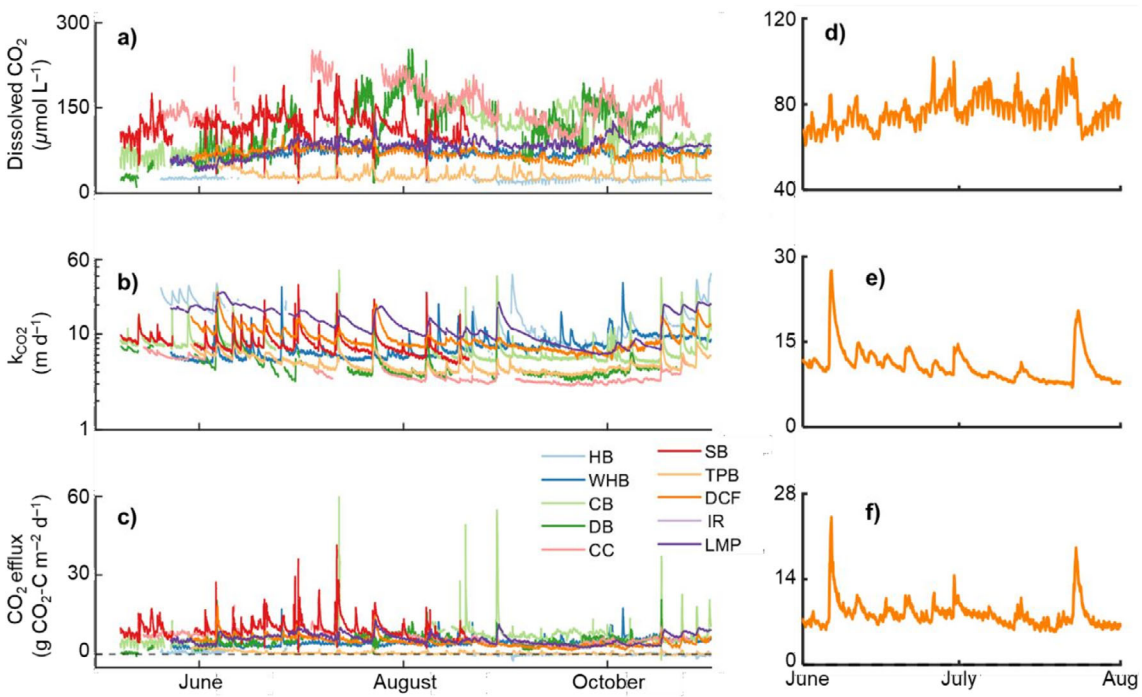

Fig. 4. Time series from 01 April 2019 to 01 November 2019 of (**a**) dissolved CO_2 concentration as measured by lotic-SIPCO2 sensors, (**b**) the calculated gas exchange rate for CO_2, k_{CO2}, on a log scale, and (**c**) the estimated rate of CO_2 emissions for all sites across the entire monitoring period. The example of (**d**) dissolved CO_2 concentration, (**e**) k_{CO2}, and (**f**) the estimated rate CO_2 emission at DCF for the period 01 May 2019 to 01 July 2019.

periods were as low as -3.8 ± 2.0 g C m^{-2} d^{-1} at HB and -3.1 ± 1.6 g C m^{-2} d^{-1} at CB. Forest cover correlated negatively with F_{CO2} as the best single predictor land cover type ($r^2 = 0.73$). Combined wetland and impervious cover explained more variability ($r^2 = 0.85$), and correlated positively with F_{CO2}.

Sensitivity and uncertainty analyses

Sensitivity analysis suggests the equations for stream velocity and the gas exchange rate (Eqs. 5, 6) are most influential in the estimation of F_{CO2} (Fig. 5). The coefficient in the calculation of k_{600} (Eq. 5) was the single most influential input variable ($|r| = 0.66$), and the other exponents and coefficients in

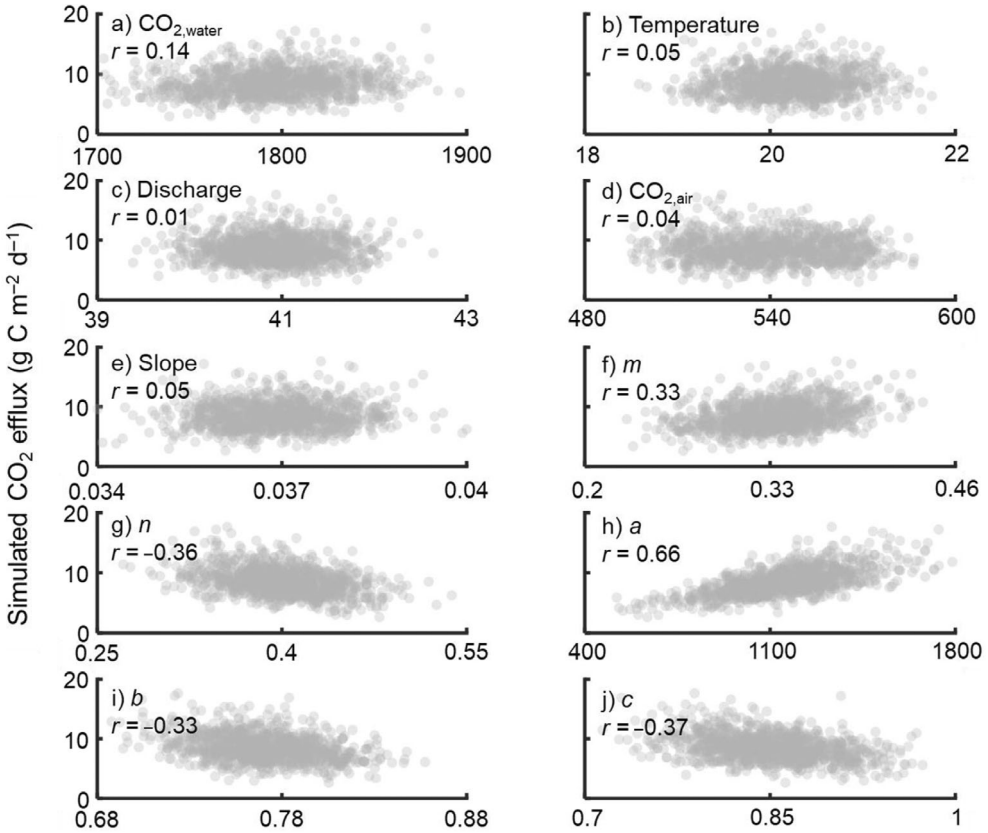

Fig. 5. Monte Carlo simulation of the sensitivity of estimating CO_2 emissions from all input variables, with results from one stream, TPB, displayed. The closer the correlation coefficient (r) is to 0, the weaker the sensitivity of the emission estimate to the selected input variable. Variables (**a**-**d**) are measured by sensors, slope (**e**) refers to the reach slope, and variables in (**f**) and (**g**) refer to Eq. 6, and (**h**-**j**) refer to Eq. 5.

the scaling of flow velocity and k_{600} are all relatively influential as well ($|r| = 0.33$–0.37). Variables measured (water temperature, air CO_2, and water CO_2) or estimated (discharge) by sensor data were relatively weak influences on estimates of F_{CO2} generally ($|r| < 0.15$). The exception to this occurs when the dissolved concentration of CO_2 approaches equilibrium with the atmosphere, for example, at HB across 2019. Here, estimation of F_{CO2} was most sensitive to the measurement of CO_2 concentration of air ($r = -0.50$) and water ($r = 0.49$). Propagating the uncertainty from these simulations, the 90% confidence interval was approximately 40% of the median F_{CO2} (i.e., 3.3 ± 1.4 g C m^{-2} d^{-1}). Site-specific uncertainty ranged from 30% of the median F_{CO2} at LMP to 58% at HB.

Across all sites, accurate estimation of the median F_{CO2} was achieved during 100% of simulations at sampling frequencies of every 2 d or more frequent (Fig. 6). Under these sampling regimes, all estimates of F_{CO2} were within the 90% confidence interval of the theoretical rate determined using the lotic-SIPCO2 and uncertainty defined above. Sampling at a weekly interval resulted in accurate estimates in more than 95% of simulations across all sites, and at a monthly interval in approximately 77% of simulations (Supporting Information Table S2).

Limiting sampling to only the daytime reduces the accuracy of these simulations. Accuracy during 100% of simulations is only achieved with daily or more frequent sampling, and at daytime monthly intervals accuracy is reduced to 64% on average. Emissions of CO_2 were on average 18% greater during nighttime compared to daytime across all sites. The difference between nighttime and daytime estimates ranging from approximately 25% higher at IR to essentially no difference at TPB and LMP. Larger differences between mean day and night emissions at a site generally led to larger uncertainty in randomly sampling daytime samples as well.

Discussion

Lotic-SIPCO2 performance

The lotic-SIPCO2 measured pCO_2 at 15-min frequency across the wide range of streams and rivers in this study, capturing patterns in CO_2 concentration, including diel cycles and interruptions to this cycle after storm events (Fig. 4). These measurements allowed for estimation and uncertainty analysis of median F_{CO2} across the sampling periods, and the effect of sampling frequency on that estimation. The design

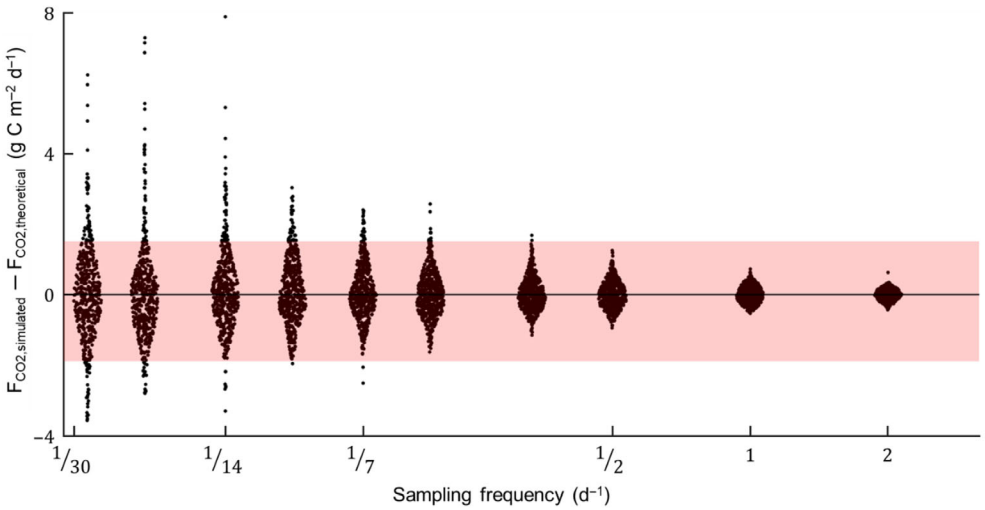

Fig. 6. The difference between simulations of the median annual rate of CO_2 emissions based on various sampling frequencies ($F_{CO2,simulated}$) and the calculated median annual rate of CO_2 emissions based on lotic-SIPCO2 measurements ($F_{CO2,theoretical}$) for DB. Sampling frequency increases left to right, from one sampling every 30 d (1/30) to two samplings per day (2). The shaded area represents the uncertainty in $F_{CO2,theoretical}$ based on analysis in this study.

combines the relatively rapid response time of headspace equilibrium methods with the increased affordability of submergible sensors (Yoon et al. 2016). The lotic-SIPCO2 equilibration time, and thus the integration time, is fast enough to reflect changes at 15-min intervals independent of flow conditions. It is theoretically possible to reduce this time even more, by reducing the tubing length further or limiting the volume of the sensor housing (e.g., adding packing material to occupy space). In addition, the lotic-SIPCO2 method benefits from the ability to calibrate the sensors in the same conditions as the measurement occurs, that is, in dry conditions because of the use of equilibrated headspace. The affordability and relatively minimal deployment requirements of the lotic-SIPCO2 raises the possibility of multiple sensor installations, therefore expanding the range of research questions that can be addressed. Given the primary source of uncertainty in calculating F_{CO2} was the estimation of gas exchange, similar to previous studies (e.g., Zappa et al. 2007), the lotic-SIPCO2 provided a robust means of pCO_2 measurement in these lotic ecosystems.

The performance of the original SIPCO2 (Hunt et al. 2017) has been favorably compared to other aquatic CO_2 sensors, suggesting the accuracy of measurement using the design presented in this study is similar (Lee et al. 2022). Indeed, the lotic-SIPCO2 measurements compared relatively well to grab samples across the streams in this study (NRMSE < 20%; Fig. 3), comparable to other evaluations of aquatic pCO_2 sensors (Yoon et al. 2016). Given the challenges with grab sample measurements of dissolved gases generally and the delayed equilibration methods in this study specifically (Jiang et al. 2014; Koschorreck et al. 2021), we expect there is some measurement error associated with our grab sample concentrations. However, we expect this source of measurement error to be relatively small given that we took preservative precautions to maximize the comparability with the sensor-derived measurements. Future evaluations of CO_2 sensors would further benefit from the development of standard methods for dissolved gas collection and analysis, as exists in the oceanographic literature (Dickson et al. 2007), especially given that regular monitoring programs are often not solely focused on dissolved gases and must balance multiple objectives. Drift was also a relatively minor, but important aspect of sensor performance, where a small minority of sensors experienced significant drift over the monitoring season. As with sensors generally, these drift determinations are a critical check on sensor accuracy over deployment periods.

Altogether, we believe the lotic-SIPCO2 provides an open-source and relatively affordable option for remote measurement of pCO_2 in lotic ecosystems. The design adaptations we describe are necessary for deployment of the lotic-SIPCO2 in streams and rivers, and address some issues potentially present in other aquatic ecosystems (i.e., biofouling). Additional variations of the SIPCO2 method were described recently which integrate wireless communication capability and alternative gas–water equilibrators (Lee et al. 2022). Combined, these adaptations offer unique and relatively affordable means of increasing CO_2 measurements across lotic ecosystems without conceding accuracy.

Some limitations are still present with the lotic-SIPCO2 and should be considered before use. First, the submerged portion of the sensor requires approximately 10 cm of water to function, limiting the ability of the lotic-SIPCO2 to function in extremely shallow environments or during particularly dry periods. This requirement is not different from submersible sensors generally. Further system modifications could be made to function in shallower systems. For example, shortening the submerged portion of the apparatus or using a horizontal pipe

as the submersible portion could offer functionality at shallower minimum depths. By selectively choosing deeper positions within the stream or river, this issue can be avoided, but does bias site selection. Placing the lotic-SIPCO2 in sufficiently deep areas also allows greater compensation depths (Colt and Bouck 1984; Aitchison et al. 2007), that is, the length over which the pumped bubble can equilibrate with the water. Some balance between the minimum depth which maintains function and the compensation depth should be considered when designing the specific application of the lotic-SIPCO2 system.

Highly turbulent streams may also require additional adaptations to the SIPCO2 to ensure a seal of the submerged portion of the sensor with the water column, which allows for headspace equilibrium to occur without interruption. Highly turbulent environments, like those of high mountain areas (Ulseth et al. 2019), could limit the effectiveness or stability of this seal by introducing bubbles or varying depth quickly. Also, the high energy nature of these streams may threaten the sensor anchoring as currently designed. For example, at the relatively urban SB, it appears a debris impact broke the anchor during one storm event in 2019 resulting in the loss of the sensor for the remainder of the monitoring season. Further modifications to the deployment setup could improve the durability, such as inserting the sensor into a well-mixed stilling well where turbulence is reduced and stability in the channel is improved.

Maintaining power supply remains a concern in heavily forested areas with dense canopies, where the continuous operation of the pump draws considerable power. The recharging of the battery with a 25 W solar panel did not suffice in some sites over monthly periods (e.g., the forested CC), and battery replacements were necessary to resume sensor function. In less-shaded areas, solar recharging was sufficient over the entire measurement season without battery replacement. The power demand from the pump appears greater than other submergible sensors (Blackstock et al. 2019), but is still less than land- or boat-based options (Yoon et al. 2016). Again, selective deployment in less-shaded areas or placement of solar panels in more advantageous positions could help overcome this limitation, as would regular battery replacements.

While greater light exposure increases the risk of biofouling, the lotic-SIPCO2 design appeared robust in limiting or preventing biofouling in the streams of this study. After implementation of the copper adaptations, biofouling did not appear to affect sensor measurement of pCO_2 at these eight locations. Cleaning procedures were maintained, whereby the tubing was brushed during roughly monthly visits, yet no visible biofilms were present. Both approaches thus appear effective, yet the application of copper tape to the inside of PVC pipes was not a trivial process. Future users should balance facilities, cost, ease, and necessity in selecting whether to use these copper adaptations and which one.

Finally, the pump mechanism of the headspace equilibration prevents the lotic-SIPCO2 from functioning in freezing environments. Freezing of the tubing through which the pump recirculates headspace air prevents circulation and can cause the pump to fail. Mechanisms of heating the sensor housing and tubing would likely increase power usage even more and could affect local biological processes and CO_2 concentration. However, a balance between intermittent heating and dissolved CO_2 measurement at reduced frequencies (e.g., twice per day) could be found to accurately estimate median F_{CO2} and limit power consumption. Because we did not implement any warming mechanisms, our study was limited to the non-freezing season.

CO_2 concentration and emissions

The streams in this study were predominantly sources of CO_2 to the atmosphere, following dominant patterns in streams and rivers globally (Lauerwald et al. 2015). The median estimated F_{CO2} (3.3 ± 1.4 g C m^{-2} d^{-1}) is comparable to those published in local (1.0 g C m^{-2} d^{-1}; Schade et al. 2016), continental (6.5 g C m^{-2} d^{-1}; Butman and Raymond 2011), and global estimates of stream and river emissions (7.9 g C m^{-2} d^{-1}; Raymond et al. 2013). Moreover, the median CO_2 concentration (64.6 ± 36.7 μM CO_2) and gas exchange rate ($k_{600} = 8.2$ m d^{-1}) fall within the measured and predicted values for this region of 170 ± 76 μM CO_2 (Herreid et al. 2020) and k_{600} from approximately 5–15 m d^{-1} (Raymond et al. 2012).

The relationships between land cover and median CO_2 concentration and emission rates also follow previous studies (Borges et al. 2018), where the importance of certain sources of CO_2 to streams and the production of CO_2 within the stream are influenced by land cover (Marescaux et al. 2018). For example, wetlands can provide a large supply of CO_2 to lotic ecosystems (Abril et al. 2014; Kirk and Cohen 2023), where CO_2 produced in wetlands is transported to streams and emitted there. Similarly, urbanization has been shown to increase riverine CO_2 emissions (Gu et al. 2021; Zhang et al. 2021), where increased inputs of nutrients and organic matter fuel in-stream production of CO_2. The stronger relationship with forest cover as a single variable may thus be more indicative of what other land covers are omitted when forest cover is high, that is, when forest cover is higher, wetland and impervious cover is lower. Further constraining the influence of land cover on stream CO_2 dynamics is important to be able to scale estimates of lotic CO_2 emissions spatially (Lauerwald et al. 2015), and data collected by high-frequency sensors systems such as the lotic-SIPCO2 can greatly aid this process through source partitioning (Marzolf et al. 2022).

Contrary to predictions (e.g., Hotchkiss et al. 2015), we do not observe a clear decrease in total F_{CO2} from smaller to larger streams. There was not a clear relationship between stream size and median F_{CO2} for the streams studied here. It may be

that land cover is a stronger influence, and thus confounding variables such as nutrients, light, and wetland cover (Bernhardt et al. 2018) almost certainly provide more complexity to predicting stream CO_2 dynamics than simply watershed size (Hutchins et al. 2020; Martinsen et al. 2020). Indeed, IR directly drains an extensive fluvial wetland, which likely explains why this stream had the highest emission rates in this study. Exploration of the influence of stream and watershed size on CO_2 emissions across a network of more uniform land cover should be aided by the affordability of the lotic-SIPCO2.

Observation of CO_2 undersaturation in general follow predictable seasonal patterns of primary productivity in streams and rivers of various sizes (Koenig et al. 2019; Savoy et al. 2019). For example, in smaller streams (e.g., CB, DB, TPB), these periods generally occurred in the spring and fall when canopy cover is minimal while solar irradiance is relatively high (Roberts et al. 2007). At the largest river (LMP), undersaturation was typically observed in the middle of summer, where canopy cover does not inhibit incident light, GPP can reach a maximum in summer (Uehlinger 2006).

The undersaturation observed at HB could be a result of sensor uncertainty. Approximately, half of measured CO_2 concentrations at HB below saturation are within the manufacturer's error of the saturation concentration. As such, the certainty of whether HB is a sink or source of CO_2 during low concentration periods is limited. The relatively high rates of turbulent gas exchange help maintain CO_2 concentration near saturation, highlighting the unique aspects of mountain streams that may alter priorities in CO_2 monitoring strategies. Assuming this undersaturation is real, it is unlikely that in-stream photosynthesis is sufficient to result in net uptake of CO_2 given the small, steep, and shaded nature of this forested watershed and the observation of undersaturation during periods of full canopy cover (Bernhardt et al. 2022). Another potential sink of CO_2 in catchments is mineral weathering (Hilton and West 2020), whereby CO_2 is geochemically consumed in the breakdown of carbonates and silicates While we do not assess the likelihood of this mechanism here, the potential for mineral weathering to act as a consequential sink of CO_2 in HB suggests a need for closer examination of watershed CO_2 sources and sinks in montane environments.

Uncertainty and sampling frequency

Uncertainty in estimating CO_2 emissions from streams and rivers is generally more sensitive to the estimation of gas exchange rather than the measurement CO_2 concentration (Fig. 5). Therefore, accurately quantifying the gas exchange rate across flow conditions will most significantly reduce uncertainty in CO_2 emission estimates. The relatively large influence of how channel geometry and velocity is scaled with discharge has been demonstrated in modeling of river processes previously (Wollheim et al. 2006, 2022), emphasizing the importance of constraining these relationships in river network studies (Bertuzzo et al. 2017; Helton et al. 2017; Koenig et al. 2019). For gas exchange, it should be possible to reduce this uncertainty with direct measurements of gas exchange across flow conditions (Hall and Ulseth 2020).

The exception to this pattern occurs when the concentration of pCO_2 approaches equilibrium with the atmosphere. In this case, the uncertainty in the measurements of pCO_2 and $CO_{2,air}$ become more important as relatively small differences in measured concentration result in large percentage differences in F_{CO2}, potentially including the difference between over- or undersaturation. For example, at HB where gas exchange rates are relatively high and CO_2 concentrations are frequently near equilibrium, the estimated F_{CO2} was most sensitive to measurements of dissolved and atmospheric CO_2. In streams like this, confidence in the CO_2 emission estimate is most improved by higher accuracy sensor systems. This could include the lotic-SIPCO2 as designed (Hunt et al. 2017; Lee et al. 2022), or additional calibration protocols, which include pressure, temperature, and humidity effects on the NDIR measurement (Martin et al. 2017) could be used during calibration and yield greater accuracy. Regardless, because the absolute F_{CO2} at these sites is frequently small, the implications for regional or continental scale carbon emission budgets are comparatively negligible.

Based on our analysis of sampling frequency, high-frequency measurements of pCO_2 are not necessary for accurate estimation of the median seasonal or annual rate of F_{CO2}. In other words, for the streams in this study, temporal variation in pCO_2 is relatively accurately captured at sampling frequencies of every 2 d. This may indicate that many studies of stream and river CO_2 emissions which rely on relatively infrequent grab sampling (Herreid et al. 2020; Gu et al. 2021) may provide a more accurate estimate of annual F_{CO2} than previously thought. However, sampling a stream every 2 d is not feasible in many circumstances. Depending on stream-specific pCO_2 diel characteristics, consideration of nighttime sampling may also be more important than sampling at a daily frequency (Gómez-Gener et al. 2021). Sites with lower median F_{CO2} generally exhibit the highest relative error in these sampling-frequency analyses, where small differences in the magnitude of emissions are a larger percentage of the mean. Thus, given a stream or river where CO_2 concentrations are near equilibrium with the atmosphere, more frequent measurements or measurement with high accuracy may be more advantageous depending on the objectives of the study, for example, to accurately estimate the mean annual F_{CO2} and downstream fluxes relative to the net carbon exchange of the catchment.

Conclusion

High-frequency monitoring of CO_2 in streams and rivers offers an unprecedented, high-temporal resolution perspective on CO_2 concentration and emission dynamics. Lotic-SIPCO2

sensors provide robust measurements of dissolved CO_2 concentration in streams at timescales necessary to delineate fine scale variability needed for a mechanistic understanding of ecosystem processes. The benefits of this sensor system include relatively fast equilibration times, affordability, ease of calibration, and limited deployment infrastructure. Effective use of the lotic-SIPCO2 method still should consider the minimum depth of the monitored stream, the available power supply, potential for biofouling, and the necessary anchoring system for the flow regime. Although high-frequency data are useful for revealing diel and storm event patterns of CO_2 concentration and emissions, they do not appear to be always necessary to accurately estimate average emission rates from streams and rivers, as observed for those in this study. If future studies find similar results in watersheds across hydroclimatic and biogeochemical regimes, then estimates of annual CO_2 emission rates which rely on daily or weekly sampling may be more confidently included in regional and global carbon budgets. Nonetheless, visiting streams to sample at daily or even weekly intervals can be difficult, therefore sensors may also be valuable for capturing these middle timescales and offer more resilience toward estimating seasonal or annual emissions. We add the lotic-SIPCO2 method as an option in this endeavor, with novel advantages for deployment in appropriate conditions.

References

Abril, G., and others. 2014. Amazon River carbon dioxide outgassing fuelled by wetlands. Nature **505**: 395–398. doi:10.1038/nature12797

Aitchison, T. F., M. B. Timmons, J. J. Bisogni, R. H. Piedrahita, and B. J. Vinci. 2007. Using oxygen gas transfer coefficients to predict carbon dioxide removal. Int. J. Recirculat. Aquac. **8**: 21–42. doi:10.21061/ijra.v8i1.1416

Battin, T. J., S. Luyssaert, L. A. Kaplan, A. K. Aufdenkampe, A. Richter, and L. J. Tranvik. 2009. The boundless carbon cycle. Nat. Geosci. **2**: 598–600. doi:10.1038/ngeo618

Bernhardt, E. S., and others. 2018. The metabolic regimes of flowing waters. Limnol. Oceanogr. **63**: S99–S118. doi:10.1002/lno.10726

Bernhardt, E. S., and others. 2022. Light and flow regimes regulate the metabolism of rivers. Proc. Natl. Acad. Sci. USA **119**: 1–5. doi:10.1073/pnas.2121976119

Bertuzzo, E., A. M. Helton, R. O. Hall, and T. J. Battin. 2017. Scaling of dissolved organic carbon removal in river networks. Adv. Water Resour. **110**: 136–146. doi:10.1016/j.advwatres.2017.10.009

Blackstock, J. M., M. D. Covington, M. Perne, and J. M. Myre. 2019. Monitoring atmospheric, soil, and dissolved CO_2 using a low-cost, Arduino monitoring platform (CO2-LAMP): Theory, fabrication, and operation. Front. Earth Sci. **7**: 1–19. doi:10.3389/feart.2019.00313

Borges, A. V., and others. 2018. Effects of agricultural land use on fluvial carbon dioxide, methane and nitrous oxide concentrations in a large European river, the Meuse (Belgium). Sci. Total Environ. **610–611**: 342–355. doi:10.1016/j.scitotenv.2017.08.047

Butman, D., and P. A. Raymond. 2011. Significant efflux of carbon dioxide from streams and rivers in the United States. Nat. Geosci. **4**: 839–842. doi:10.1038/ngeo1294

Butman, D., and others. 2018. Chapter 14: Inland waters, p. 568–595. *In* Second state of the carbon cycle report. doi:10.7930/SOCCR2.2018.Ch14

Cole, J. J., and others. 2007. Plumbing the global carbon cycle: Integrating inland waters into the terrestrial carbon budget. Ecosystems **10**: 171–184. doi:10.1007/s10021-006-9013-8

Colt, J., and G. Bouck. 1984. Design of packed columns for degassing. Aquac. Eng. **3**: 251–273. doi:10.1016/0144-8609(84)90007-4

Crawford, J. T., E. H. Stanley, M. M. Dornblaser, and R. G. Striegl. 2017. CO_2 time series patterns in contrasting headwater streams of North America. Aquat. Sci. **79**: 473–486. doi:10.1007/s00027-016-0511-2

Dickson, A. G., C. L. Sabine, and J. R. Christian. 2007. Guide to best practices for ocean CO_2 measurements. North Pacific Marine Science Organization, PICES Special Publication.

Dinsmore, K. J., and M. F. Billett. 2008. Continuous measurement and modeling of CO_2 losses from a peatland stream during stormflow events. Water Resour. Res. **44**: 1–11. doi:10.1029/2008WR007284

Dinsmore, K. J., M. B. Wallin, M. S. Johnson, M. F. Billett, K. Bishop, J. Pumpanen, and A. Ojala. 2013. Contrasting CO_2 concentration discharge dynamics in headwater streams: A multi-catchment comparison. J. Geophys. Res. Biogeosci. **118**: 445–461. doi:10.1002/jgrg.20047

Drake, T. W., P. A. Raymond, and R. G. M. Spencer. 2018. Terrestrial carbon inputs to inland waters: A current synthesis of estimates and uncertainty. Limnol. Oceanogr. Lett. **3**: 132–142. doi:10.1002/lol2.10055

Emery, N. J., and A. C. Greenville. 2015. Gathering lots of data on a small budget. Science **353**: 1360–1361. doi:10.1126/science.aag305

Gómez-Gener, L., and others. 2021. Global carbon dioxide efflux from rivers enhanced by high nocturnal emissions. Nat. Geosci. **14**: 289–294. doi:10.1038/s41561-021-00722-3

Gu, C., S. Waldron, and A. M. Bass. 2021. Carbon dioxide, methane, and dissolved carbon dynamics in an urbanized river system. Hydrol. Process. **35**: 1–17. doi:10.1002/hyp.14360

Hall, R. O., and H. L. Madinger. 2018. Use of argon to measure gas exchange in turbulent mountain streams. Biogeosciences **15**: 3085–3092. doi:10.5194/bg-15-3085-2018

Hall, R. O., and A. J. Ulseth. 2020. Gas exchange in streams and rivers. WIREs Water **7**: 1–19. doi:10.1002/wat2.1391

Haque, M. M., M. S. Begum, O. K. Nayna, S. M. Tareq, and J. H. Park. 2022. Seasonal shifts in diurnal variations of pCO2 and O2 in the lower Ganges River. Limnol. Oceanogr. Lett. **7**: 191–201. doi:10.1002/lol2.10246

Helton, A. M., R. O. Hall, and E. Bertuzzo. 2017. How network structure can affect nitrogen removal by streams. Freshw. Biol. **63**: 1–13. doi:10.1111/fwb.12990

Herreid, A. M., A. S. Wymore, R. K. Varner, and W. H. McDowell. 2020. Divergent controls on stream greenhouse gas concentrations across a land use gradient. Ecosystems: 1–50. doi:10.1007/s10021-020-00584-7

Hilton, R. G., and A. J. West. 2020. Mountains, erosion and the carbon cycle. Nat. Rev. Earth Environ. **1**: 284–299. doi:10.1038/s43017-020-0058-6

Hotchkiss, E. R., R. O. Hall Jr., R. A. Sponseller, D. Butman, J. Klaminder, H. Laudon, M. Rosvall, and J. Karlsson. 2015. Sources of and processes controlling CO_2 emissions change with the size of streams and rivers. Nat. Geosci. **8**: 696–699. doi:10.1038/ngeo2507

Hunt, C. W., L. Snyder, J. E. Salisbury, D. Vandemark, and W. H. McDowell. 2017. SIPCO2: A simple, inexpensive surface water pCO_2 sensor. Limnol. Oceanogr. Methods **15**: 291–301. doi:10.1002/lom3.10157

Hutchins, R. H. S., J. P. Casas-Ruiz, Y. T. Prairie, and P. A. del Giorgio. 2020. Magnitude and drivers of integrated fluvial network greenhouse gas emissions across the boreal landscape in Québec. Water Res. **173**: 115556. doi:10.1016/j.watres.2020.115556

Jiang, Z. P., and others. 2014. Application and assessment of a membrane-based pCO2 sensor under field and laboratory conditions. Limnol. Oceanogr. Methods **12**: 264–280. doi:10.4319/lom.2014.12.264

Johnson, M. S., M. F. Billett, K. J. Dinsmore, M. Wallin, K. E. Dyson, and R. S. Jassal. 2010. Direct and continuous measurement of dissolved carbon dioxide in freshwater aquatic systems—Method and applications. Ecohydrology **3**: 68–78. doi:10.1002/eco.95

Kirk, L., and M. J. Cohen. 2023. River corridor sources dominate CO_2 emissions from a lowland river network. J. Geophys. Res. Biogeosci. **128**: 1–17. doi:10.1029/2022jg006954

Knighton, D. 1998. Fluvial forms and processes: A new perspective. 1st ed. Hodder Arnold.

Koenig, L. E. 2017. Hydrological and biogeochemical controls on carbon and nitrogen export from river networks. Univ. of New Hampshire.

Koenig, L. E., M. D. Shattuck, L. E. Snyder, J. D. Potter, and W. H. McDowell. 2017. Deconstructing the effects of flow on DOC, nitrate, and major ion interactions using a high-frequency aquatic sensor network. Water Resour. Res. **53**: 655–673. doi:10.1002/2017WR020739

Koenig, L. E., A. M. Helton, P. Savoy, E. Bertuzzo, J. B. Heffernan, R. O. Hall, and E. S. Bernhardt. 2019. Emergent productivity regimes of river networks. Limnol. Oceanogr. Lett. **4**: 173–181. doi:10.1002/lol2.10115

Koschorreck, M., Y. T. Prairie, J. Kim, and R. Marcé. 2021. Technical note: CO_2 is not like CH_4—Limits of and corrections to the headspace method to analyse pCO_2 in fresh water. Biogeosciences **18**: 1619–1627. doi:10.5194/bg-18-1619-2021

Lauerwald, R., G. G. Laurelle, J. Hartmann, P. Ciais, and P. A. G. Regnier. 2015. Spatial patterns in CO_2 evasion from the global river network. Global Biogeochem. Cycl. **29**: 534–554. doi:10.1002/2014GB004941

Lee, D. J. J., K. T. Kek, W. W. Wong, M. S. Mohd Nadzir, J. Yan, L. Zhan, and S. C. Poh. 2022. Design and optimization of wireless in-situ sensor coupled with gas–water equilibrators for continuous pCO_2 measurement in aquatic environments. Limnol. Oceanogr. Methods **20**: 500–513. doi:10.1002/lom3.10500

Liu, S., and P. A. Raymond. 2018. Hydrologic controls on pCO_2 and CO_2 efflux in US streams and rivers. Limnol. Oceanogr. Lett. **3**: 428–435. doi:10.1002/lol2.10095

Magen, C., L. L. Lapham, J. W. Pohlman, K. Marshall, S. Bosman, M. Casso, and J. P. Chanton. 2014. A simple headspace equilibration method for measuring dissolved methane. Limnol. Oceanogr. Methods **12**: 637–650. doi:10.4319/lom.2014.12.637

Marescaux, A., V. Thieu, A. V. Borges, and J. Garnier. 2018. Seasonal and spatial variability of the partial pressure of carbon dioxide in the human-impacted Seine River in France. Sci. Rep. **8**: 1–14. doi:10.1038/s41598-018-32332-2

Martin, C. R., N. Zeng, A. Karion, R. R. Dickerson, X. Ren, B. N. Turpie, and K. J. Weber. 2017. Evaluation and environmental correction of ambient CO2 measurements from a low-cost NDIR sensor. Atmos. Meas. Tech. **10**: 2383–2395. doi:10.5194/amt-10-2383-2017

Martinsen, K. T., T. Kragh, and K. Sand-Jensen. 2020. Carbon dioxide partial pressure and emission throughout the Scandinavian stream network. Global Biogeochem. Cycl. **34**: 1–14. doi:10.1029/2020GB0067036

Marzolf, N. S., G. E. Small, D. Oviedo-Vargas, C. N. Ganong, J. H. Duff, A. Ramírez, C. M. Pringle, D. P. Genereux, and M. Ardón. 2022. Partitioning inorganic carbon fluxes from paired O_2-CO_2 gases in a headwater stream, Costa Rica. Biogeochemistry **160**: 259–273. doi:10.1007/s10533-022-00954-4

Morse, N. B., and W. M. Wollheim. 2014. Climate variability masks the impacts of land use change on nutrient export in a suburbanizing watershed. Biogeochemistry **121**: 45–59. doi:10.1007/s10533-014-9998-6

Mulholland, P. J., H. M. Valett, J. R. Webster, S. A. Thomas, L. W. Cooper, S. K. Hamilton, and B. J. Peterson. 2004. Stream denitrification and total nitrate uptake rates measured using a field ^{15}N tracer addition approach. Limnol. Oceanogr. **49**: 809–820. doi:10.4319/lo.2004.49.3.0809

Natchimuthu, S., M. B. Wallin, L. Klemedtsson, and D. Bastviken. 2017. Spatio-temporal patterns of stream methane and carbon dioxide emissions in a hemiboreal catchment in Southwest Sweden. Sci. Rep. **7**: 1–12. doi:10.1038/srep39729

Pelletier, P. M. 1988. Uncertainties in the single determination of river discharge: A literature review. Can. J. Civ. Eng. **15**: 834–850. doi:10.1139/l88-109

Peter, H., G. A. Singer, C. Preiler, P. Chifflard, G. Steniczka, and T. J. Battin. 2014. Scales and drivers of temporal pCO_2 dynamics in an Alpine stream. J. Geophys. Res. Biogeosci. **119**: 1078–1091. doi:10.1002/2013JG002552

Pontius, R. G., O. Thontteh, and H. Chen. 2008. Components of information for multiple resolution comparison between maps that share a real variable. Environ. Ecol. Stat. **15**: 111–142. doi:10.1007/s10651-007-0043-y

Ranatunga, T., S. T. Y. Tong, and Y. J. Yang. 2017. An approach to measure parameter sensitivity in watershed hydrological modelling. Hydrol. Sci. J. **62**: 76–92. doi:10.1080/02626667.2016.1174335

Raymond, P. A., C. J. Zappa, D. Butman, T. L. Bott, J. Potter, P. Mulholland, A. E. Laursen, W. H. Mcdowell, and D. Newbold. 2012. Scaling the gas transfer velocity and hydraulic geometry in streams and small rivers. Limnol. Oceanogr. Fluids Environ. **2**: 41–53. doi:10.1215/21573689-1597669

Raymond, P. A., and others. 2013. Global carbon dioxide emissions from inland waters. Nature **503**: 355–359. doi:10.1038/nature12760

Reed, A. P., E. G. Stets, S. F. Murphy, and E. A. Mullins. 2021. Aquatic-terrestrial linkages control metabolism and carbon dynamics in a mid-sized, urban stream influenced by snowmelt. doi:10.1029/2021JG006296

Richardson, M., R. D. Moore, and A. Zimmermann. 2017. Variability of tracer breakthrough curves in mountain streams: Implications for streamflow measurement by slug injection. Can. Water Resour. J. **42**: 21–37. doi:10.1080/07011784.2016.1212676

Riml, J., A. Campeau, K. Bishop, and M. B. Wallin. 2019. Spectral decomposition reveals new perspectives on CO_2 concentration patterns and soil-sream linkages. J. Geophys. Res. Biogeosci. **124**: 3039–3056. doi:10.1029/2018JG004981

Roberts, B. J., P. J. Mulholland, and W. R. Hill. 2007. Multiple scales of temporal variability in ecosystem metabolism rates: Results from 2 years of continuous monitoring in a forested headwater stream. Ecosystems **10**: 588–606. doi:10.1007/s10021-007-9059-2

Robison, A. L., W. M. Wollheim, C. R. Perryman, A. R. Cotter, J. E. Mackay, R. K. Varner, P. Clarizia, and J. G. Ernakovich. 2022. Dominance of diffusive methane emissions from lowland headwater streams promotes oxidation and isotopic enrichment. Front. Environ. Sci. **9**: 1–14. doi:10.3389/fenvs.2021.791305

Rocher-Ros, G., R. A. Sponseller, A. K. Bergström, M. Myrstener, and R. Giesler. 2020. Stream metabolism controls diel patterns and evasion of CO_2 in Arctic streams. Glob. Change Biol. **26**: 1400–1413. doi:10.1111/gcb.14895

Rode, M., and others. 2016. Sensors in the stream: The high-frequency wave of the present. Environ. Sci. Tech. **50**: 10297–10307. doi:10.1021/acs.est.6b02155

Savoy, P., A. P. Appling, J. B. Heffernan, E. G. Stets, J. S. Read, J. W. Harvey, and E. S. Bernhardt. 2019. Metabolic rhythms in flowing waters: An approach for classifying river productivity regimes. Limnol. Oceanogr. **64**: 1835–1851. doi:10.1002/lno.11154

Sawakuchi, H. O., and others. 2017. Carbon dioxide emissions along the lower Amazon River. Front. Mar. Sci. **4**: 1–12. doi:10.3389/fmars.2017.00076

Schade, J. D., J. Bailio, and W. H. McDowell. 2016. Greenhouse gas flux from headwater streams in New Hampshire, USA: Patterns and drivers. Limnol. Oceanogr. **61**: S165–S174. doi:10.1002/lno.10337

Uehlinger, U. 2006. Annual cycle and inter-annual variability of gross primary production and ecosystem respiration in a floodprone river during a 15-year period. Freshw. Biol. **51**: 938–950. doi:10.1111/j.1365-2427.2006.01551.x

Ulseth, A. J., R. O. Hall, M. Boix Canadell, H. L. Madinger, A. Niayifar, and T. J. Battin. 2019. Distinct air–water gas exchange regimes in low- and high-energy streams. Nat. Geosci. **12**: 259–263. doi:10.1038/s41561-019-0324-8

van Geldern, R., P. Schulte, M. Mader, A. Baier, and J. A. C. Barth. 2015. Spatial and temporal variations of pCO_2, dissolved inorganic carbon and stable isotopes along a temperate karstic watercourse. Hydrol. Process. **29**: 3423–3440. doi:10.1002/hyp.10457

Wallin, M. B., J. Audet, M. Peacock, E. Sahlée, and M. Winterdahl. 2020. Carbon dioxide dynamics in an agricultural headwater stream driven by hydrology and primary production. Biogeosciences **17**: 2487–2498. doi:10.5194/bg-17-2487-2020

Welles, J. M., and D. K. McDermitt. 2005. Measuring carbon dioxide in the atmosphere. *In* J. L. Hatfield and J. M. Baker [eds.], Micrometeorology in agricultural systems. doi:10.2134/agronmonogr47.c13

Wieczorek, M. E., S. E. Jackson, and G. E. Schwarz. 2018. Select attributes for NHDPlus version 2.1 reach catchments and modified network routed upstream watersheds for the conterminous United States (Ver. 3.0 January 2021). U.S. Geological Survey data release. doi:10.5066/F7765D7V

Wollheim, W. M., C. J. Vörösmarty, B. J. Peterson, S. P. Seitzinger, and C. S. Hopkinson. 2006. Relationship between river size and nutrient removal. Geophys. Res. Lett. **33**: 2–5. doi:10.1029/2006GL025845

Wollheim, W. M., R. J. Stewart, G. R. Aiken, K. D. Butler, N. B. Morse, and J. Salisbury. 2015. Removal of terrestrial DOC in aquatic ecosystems of a temperate river network. Geophys. Res. Lett. **42**: 6671–6679. doi:10.1002/2015GL064647

Wollheim, W. M., G. K. Mulukutla, C. Cook, and R. O. Carey. 2017. Aquatic nitrate rentention at river network scales across flow conditions determined using nested in situ sensors. Water Resour. Res. **53**: 9740–9756. doi:10.1002/2017WR020644

Wollheim, W. M., T. K. Harms, A. L. Robison, L. E. Koenig, A. M. Helton, C. Song, W. B. Bowden, and J. C. Finlay. 2022. Superlinear scaling of riverine biogeochemical function with watershed size. Nat. Commun. **13**: 1–9. doi:10.1038/s41467-022-28630-z

Yanai, R. D., and others. 2015. Sources of uncertainty in estimating stream solute export from headwater catchments at three sites. Hydrol. Process. **29**: 1793–1805. doi:10.1002/hyp.10265

Yoon, T. K., H. Jin, N. H. Oh, and J. H. Park. 2016. Technical note: Assessing gas equilibration systems for continuous pCO_2 measurements in inland waters. Biogeosciences **13**: 3915–3930. doi:10.5194/bg-13-3915-2016

Zappa, C. J., W. R. McGillis, P. A. Raymond, J. B. Edson, E. J. Hintsa, H. J. Zemmelink, J. W. H. Dacey, and D. T. Ho. 2007. Environmental turbulent mixing controls on air–water gas exchange in marine and aquatic systems. Geophys. Res. Lett. **34**: 1–6. doi:10.1029/2006GL028790

Zhang, W., H. Li, Q. Xiao, and X. Li. 2021. Urban rivers are hotspots of riverine greenhouse gas (N_2O, CH_4, CO_2) emissions in the mixed-landscape Chaohu lake basin. Water Res. **189**: 116624. doi:10.1016/j.watres.2020.116624

Acknowledgments

We thank Brian Saccardi for his help in constructing sensors and Stanley Glidden for his assistance in developing Fig. 1. We would like to thank the two reviewers for their thoughtful and constructive input on this manuscript. This work was partially funded by PIE-LTER OCE-1637630, EF-1926423, EF-1926591, the NSF Established Program to Stimulate Competitive Research (EPSCoR 1101245), NSF SRS 2215300, and a Graduate Research Fellowship to L.E. K. (GRFP-0913620). Partial support was provided by the New Hampshire Agricultural Experiment Station (NHAES) through USDA National Institute of Food and Agriculture (NIFA) Hatch Project 0225006 to W.M.W., scientific contribution 3003, and NIFA McIntire Stennis Project 1019522 to W.H.M. Partial funding was also provided from the University of New Hampshire Natural Resources and Earth Systems Science program. Open access funding provided by Ecole Polytechnique Federale de Lausanne.

Submitted 01 June 2023
Revised 04 December 2023
Accepted 15 January 2024

Associate editor: Mike DeGrandpre